Oregon Undergraduate Research Journal
1.1 (2011) ISSN: 2160-617X (online)
http://journals.oregondigital.org/ourj/
DOI: 10.5399/uo/ourj.1.1.1551

Forward Modeling to Assess and Improve Gravity Network Geometry at Kilauea Volcano, Hawai`i

Patricia MacQueen, Department of Geological Sciences, University of Oregon

Abstract

Scientists have been using campaign gravity surveys to monitor volcanic activity at Kilauea's summit for decades, yet we have a poor understanding of the ability of the existing network to resolve sources of magma accumulation with different mass changes and depths. We also do not yet have a fully quantified measure of the relative importance of the stations in the network. This research tests the network using a simple forward modeling approach over a range of likely source volumes and depths. The analysis determines network sensitivity to three different likely source locations, calculates the relative importance of stations in the network, and examines the problem of signal distortion imposed by network geometry. This work finds that the current network is least sensitive to south caldera sources, and investigates the location and number of stations that will resolve this problem most effectively.

Introduction

Measurements of gravity changes at the summit of a volcano can yield valuable information about subsurface mass movements as magma rises toward the surface. However, how well the network of gravity monitoring stations resolves these changes in mass determines the value of the information a campaign gravity survey provides. A campaign gravity survey measures changes in gravitational acceleration over time at a network of gravity stations whose locations remain constant for all surveys. Since gravitational acceleration is determined by the distribution of mass in the subsurface, measuring the change in gravity over time at these gravity stations gives researchers an idea of mass change over time. Ideally, such a network of stations would be arranged on a grid, to minimize spatial signal distortion that arises from irregular grid spacing. Unfortunately, this is usually effectively impossible due to the complex topography around an active volcano and considerations of time and money. A network has existed on the summit of Kilauea Volcano in Hawaii, United States, for decades (Johnson et al., 2010). Gravity stations are co-located with an existing and more extensive network of benchmarks used for annual leveling surveys.

Kilauea Volcano is a shield volcano located at the southeastern end of the Hawaiian volcanic chain on the island of Hawai'i (Figure 1). Kilauea has been erupting continuously since 1983; its most recent phase of eruption consists of a summit lava lake, a lava pond at Pu`u O`o, effusive

flank eruptions, and a new fissure eruption near Napa`au crater ("HVO Kilauea Status Page," May 2011).

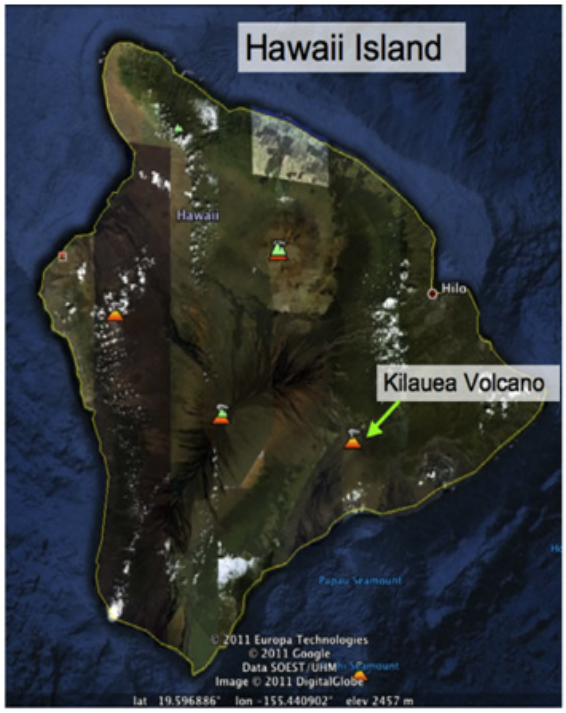

Figure 1. Map of Hawai'i Island with the location of Kilauea Volcano marked.

Although its eruptions are primarily effusive, the United States Geological Survey (USGS) considers Kilauea to be the most dangerous volcano in the United States because of its ongoing activity and the high potential for persons and property to be exposed to volcanic activity from Kilauea and the volcano's east rift zone. The many tourists who flock to Kilauea make hazard mitigation at the volcano difficult (Ewert et al., 2005). In addition to effusive eruptions, Kilauea has erupted explosively in the past. Kilauea's caldera formed in a massive eruption in the 16th century, killed visitors to the caldera in an explosive eruption in 1924, and more recently, a smaller explosion in March 2008 accompanied the formation of the current lava column in Halema`uma`u (Jaggar, 1924; Swanson, 2008; Poland et al., 2009; Fee et al., 2010; Houghton et al., 2011). Recent research has uncovered several other explosive eruptions in Kilauea's history, including an eruption that left tephra sheets blanketing the south caldera region, producing what is known as the Kulanaokuaiki tephra (Fiske et al., 2009). Less dramatic than these explosive eruptions but no less concerning is "vog" (volcanic fog). The gas plume from Kilauea's current summit eruption, full of noxious sulfur dioxide, trails westward over the Kailua-Kona area, creating vog which causes many respiratory problems (Sutton et al., 2000).

Eruptive events at Kilauea are commonly preceded by months to years of magma accumulation in a buried magma reservoir beneath the summit. During eruptive events, this magma drains rapidly, sometimes in a matter of hours, to erupt from vents on the volcano's rift zones. Most monitoring efforts at Kilauea are focused on the summit area as it is theorized that

this is where magma rises from great depths through the crust and into the volcanic edifice (Decker, 1987; Johnson, 1987). GPS, leveling, tilt, seismographic, and gravity instruments all monitor these inflation and deflation events.

Using gravity to monitor volcanoes is crucial for constraining other data sources and providing greater advance warning. Because gravity detects changes in mass, it provides an important constraint on the ascent of magma. The gravitational acceleration measured at any one point on the surface of the earth depends on the distribution of mass around that point. Accordingly, by measuring gravitational acceleration at several points in a given area, we can gain some idea of what lies beneath the surface. If we do such surveys repeatedly in the same area using the same measurement points we can detect changes in gravitational acceleration over time. Changes in gravitational acceleration allow us to detect changes in the distribution of mass over time (Dzurisin, 2007; Battaglia et al., 2008). Gravitational acceleration is determined by either continuous, permanent meters or a series of campaign measurements. A continuous gravity meter gives better temporal resolution but the limited number of stations gives poor spatial resolution. The number of continuous meters is limited by the substantial bunkers needed to protect a meter running continuously in an active volcanic region. A campaign gravity survey consists of many single, discrete measurements of gravity at a set network of benchmarks, which are then repeated at a given interval, usually every few months or years. This method gives better spatial resolution but poor temporal resolution, since surveys are time intensive and performed infrequently, but the campaign stations cover a wider spatial area than is possible with continuous meters (Battaglia et al., 2008).

The distribution of mass that produces a given gravity signal is non-unique, as is the distribution of volume change that produces a deformation signal. Coupling the two independent observations can better resolve the source. Interpretation of deformation data, in turn, benefits from gravity data, as gravity data can help constrain the source of deformation. Deformation can tell us that something is inflating, its location, and its volume, but it cannot tell us anything about the source's density, which can be a key factor in establishing the identity of the source (e.g. magma or hydrothermal). For example, gravity studies at Long Valley Caldera were able to determine that a source of inflation was from basaltic magma saturated with hydrothermal fluids, rather than hydrothermal fluids alone, which has vastly different hazard implications. Hydrothermal activity is typically harmless to humans, whereas the presence of basaltic magma may imply an eruption is possible in the near future (Battaglia et al., 1999, 2003).

On Hawai'i, a gravity survey could help distinguish between a source that is inflating from subsurface accumulation of magma versus a source that is inflating due to vesiculation of an existing magma body. Figure 2 depicts the hypothetical results from gravity and deformation surveys under these two scenarios. In the former scenario, a deformation survey and a gravity survey across the source would show an increase in gravity and uplift at the source, indicating both an increase in volume and an increase in mass from the addition of magma. In the latter scenario, a deformation survey across the source would show an increase in uplift at the source, but a gravity survey (after corrections for the change in elevation) would show no change,

indicating a volume increase without a corresponding increase in mass. This would suggest a decrease in density of source, possibly from vesiculation (Figure 2).

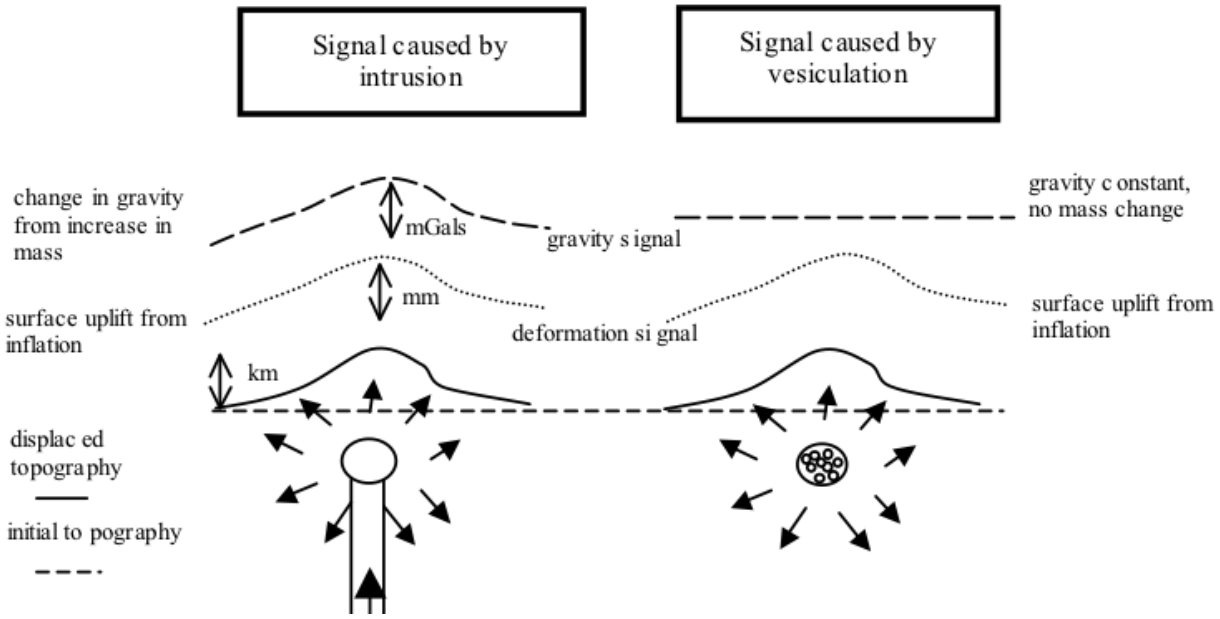

Figure 2. On the left, an intrusion causes increases in gravity and uplift in deformation across the source. On the right, a vesiculating source causes uplift across the source, but no change in gravity.

From a monitoring standpoint, changes in gravity are sometimes detectable long before other more traditional precursors. During a volcanic crisis on the island of Fogo, a subsurface accumulation of magma was detected through campaign gravity surveys months before changes in deformation or seismic activities were detected (Fonseca et al., 2003). Gravity data can also help to clarify the eruption mechanism. During a flank eruption on Mt. Etna, a continuous gravity meter recorded a sharp decrease in gravity, followed by a sudden but more gradual increase in gravity. With this continuous gravity data, seismic data, and petrological evidence, scientists were able to deduce that the mechanism for this flank eruption was a dry fault opening in the volcanic edifice, which then created a path for magma to erupt at the surface (Carbone et al., 2007). Studies at Campi Flegrei, Mayasa, and Merapi have also used gravity to monitor volcanic activity (Jousset et al., 2000; Gottsmann et al., 2003; Camacho et al., 2007; Battaglia et al., 2008; Williams-Jones et al., 2003, 2008). At Kilauea, work by Daniel Johnson suggested that long-term subsidence at the summit may be due to deflation of magma bodies through gas release. Gravity measurements would be crucial to distinguish this activity from the rapid deflation associated with eruptions on the rift zones (Johnson, 1992).

My primary objectives for this study are to assess the capabilities of the current network geometry and suggest improvements where necessary. Kilauea's complex volcanic terrain limits station location, so it is important to understand the capabilities of a gravity network on the summit, given the limitations on station location and density. I will determine network capabilities by examining the minimum depth and volume combinations necessary for the

network to detect a source. I will also examine the relative importance of the different stations in the network. Since network geometry can distort a spatial signal, I will also look at this problem for Kilauea's network. Using what I know about network capabilities, I will suggest improvements as needed.

Methods

Gravity monitoring at Kilauea currently consists of two continuous gravity meters and a network of campaign gravity benchmarks that are co-located with leveling benchmarks for height control. These campaign gravity benchmarks are typically located along paved roads for easy access and surveying, with exceptions including a small loop of benchmarks in the caldera northeast of Halema`uma`u crater and three stations in the south caldera region (Figure 3).

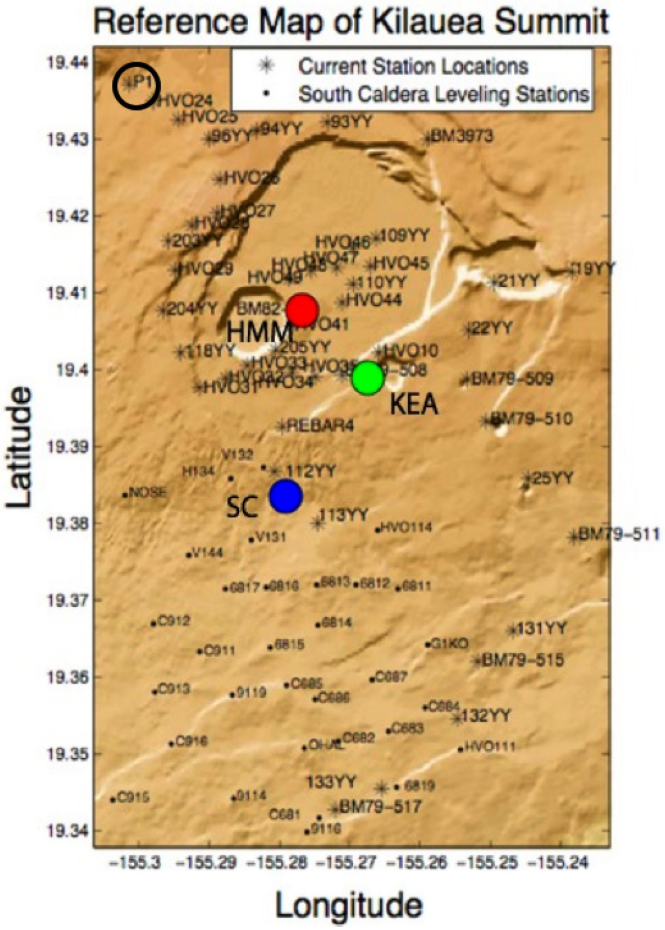

Figure 3. Reference map of gravity and deformation stations in the summit area. Current gravity stations are marked with stars, and deformation stations in the south caldera region are marked with dots. The three colored dots represent source locations for this study. P1, the base station, is circled in black.

In an actual campaign gravity survey, gravity values for all stations are calculated relative to P1, a benchmark presumed to be stable relative to the volcano. These benchmarks are surveyed using the double-loop method: first the base station (P1) is surveyed, followed by a few stations,

the base station again, the same stations as before, and finally the base station a third time to end the day's survey. Gravity meters drift over time, such that a reading at a stable benchmark early in the day will be lower than a reading at the same benchmark later in the day. This effect increases with time. Surveying the base station three times constrains the drift of the instrument as well as permitting an error calculation for each station. Each survey day is as short as possible, as long survey days mean larger drift on the meter. For the campaign gravity surveys, HVO uses a Scintrex CG5 relative gravity meter, which (under Kilauea field conditions) has an error of approximately 15μGal (1 Gal is equal to 1 cm/s^2).

To test the capabilities of the current network of campaign gravity benchmarks, I forward modeled a series of very simple scenarios. The simplest possible model for magma accumulation and withdrawal uses an analytical point source. An analytical model relies on simple equations and is useful because it is computationally simpler and thus requires minimal computing power and time. Although a point source does not accurately represent volcanic activity at Kilauea, it is a computationally simple model that actually fits real data quite well in many cases (Battaglia et al., 2008). My model uses equations for a point source of expansion and contraction in an elastic half-space adapted from Mogi (Dzurisin, 2007). I assumed a density of 2800 kg/m^3 for basaltic magma, and a density of 3100 kg/m^3 for basaltic crust. The total gravity change is calculated as follows (Figure 4):

$$\Delta g = \frac{G\Delta V d}{\left(r^2 + d^2\right)^{3/2}}\left[\left(\rho_m - \rho_c\right) + 2\rho_c\left(1-\nu\right) + \rho_c\left(1-2\nu\right)\right]$$

Figure 4. The analytical equations used in my model, adapted from a basic Mogi model.

where Δg is gravity change, G is the gravitational constant, ΔV is the change in volume of the source, d is the depth of the source, r is the radial distance to the source, $\boldsymbol{\rho}_m$ is the density of magma, $\boldsymbol{\rho}_c$ is the density of the crust, and ν is Poisson's ratio (2.5). The first term in the brackets calculates gravity change due to the increase in mass. The second term calculates gravity change due to uplift of the inflating point source. The third term calculates gravity change due to the elastic expansion of the crust changing the density of the crust (Dzurisin, 2007).

A cross section of gravity change across a Mogi source shows a steady increase in gravity as horizontal distance to the source approaches zero (Figure 5). Gravity reaches a peak above the source location (Figure 5). As the source gets more shallow, the peak becomes sharper, and as the source becomes larger in volume the whole curve moves up.

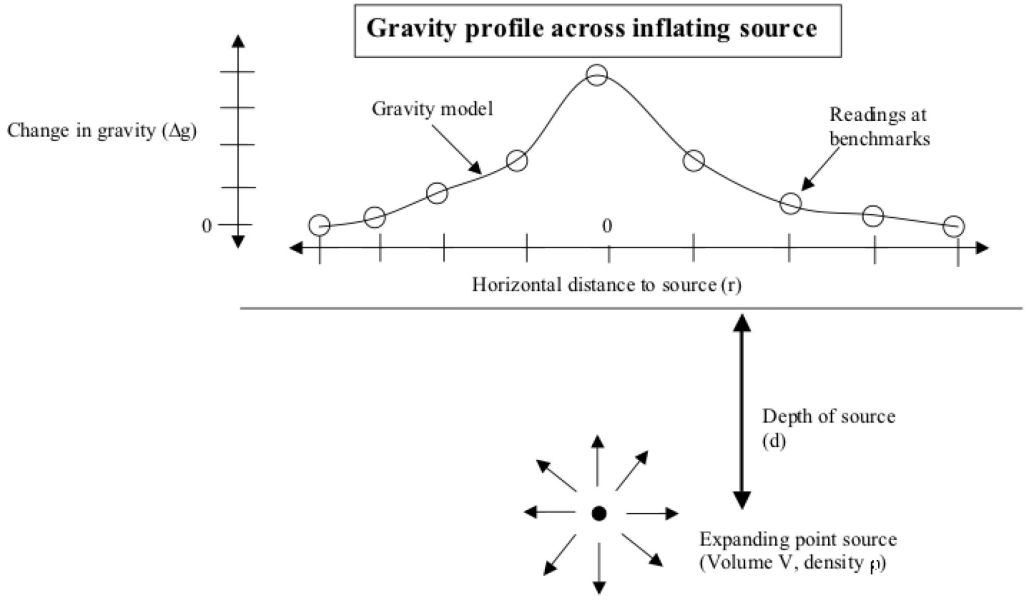

Figure 5. Change in gravity versus distance from source for an expanding point source (Mogi model). The curve peaks smoothly above the source, and the sharpness of the peak increases as the source depth decreases.

In map view, the signal from a Mogi source is radially symmetric about the source location (Figure 6).

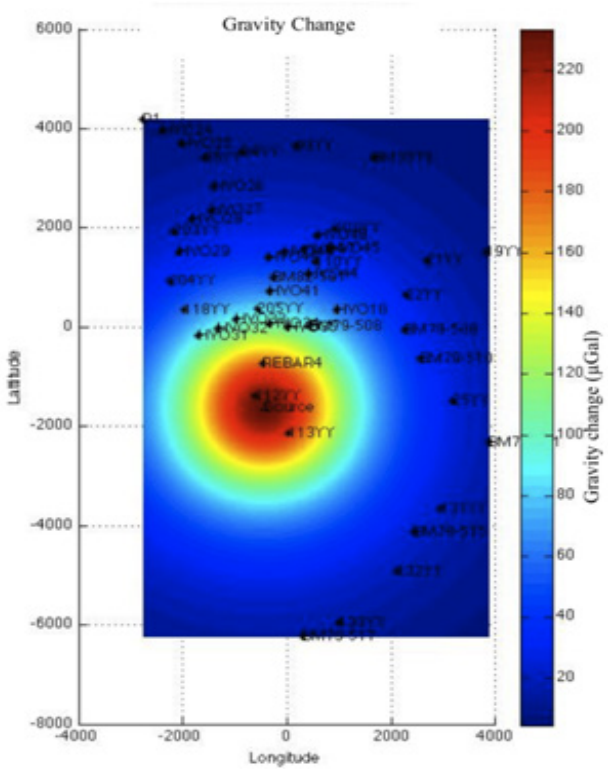

Figure 6. Map view of an expanding Mogi source. Note how gravity change is greatest over the source and decreases uniformly with distance from the source.

For this study, I focused on three source areas: Halema`uma`u crater (HMM), Keanakakoi crater (KEA), and the South Caldera (SC) region (near station 112YY), all known areas of magma storage (Decker, 1987; Johnson, 1987; Johnson, 1992; Johnson et al., 2010) (Figure 3). Most recently there has been inflation and deflation at HMM, and deflation at SC (Johnson et al., 2010). Inflation and deflation episodes have also occurred at KEA in the past few decades of observation (Decker, 1987). Whether or not the gravity change at the stations in the existing network is above the noise level of the gravimeter can be a way to assess network capabilities quantitatively.

Under Kilauea field conditions, the noise level of the Scintrex CG5 spring gravimeters used at HVO is about 15 μGal. If the model calculates a gravity change at a station that is above 15 μGal, this measurement is considered reliable and useful. If it is below 15 μGal, it is not, because the measurement cannot be distinguished from the noise of the meter. The number of stations above this noise level for a given depth and volume of source provides a measure of how well the network detects that source. Accordingly, to assess the effectiveness of the network, I ran a series of inflation simulations over a range of depth (0 to 10 km) and volume ($5.5x10^5$ to 10^9 m^3) combinations. For each volume/depth pair, I kept track of how many stations were above the noise level for each simulation and of how many times each individual station was above the noise level over all the simulations. To quantify station value, I established a ranking system based on how many times each individual station measured above the noise level. I ran different depth/volume simulations for each of the three sources, and then added these results to get a cumulative result in addition to the results from each individual source. For each of these four data sets (three single sources and one cumulative), I identified the highest score (number of times a station measured above the noise level), and called this the "best possible value" (BPV). I then arbitrarily decided that stations that scored over 80% of the BPV in that data set were important stations, and those that scored below 80% were less important. This arbitrary cutoff was based on map-view contours of station scores. Each map had 5 to 6 contours spaced evenly between the lowest and highest score. As the third contour (roughly half way between highest and lowest score) usually fell close to 80% of the BPV, I decided this would be an acceptable cutoff point.

To gain some understanding of how the network geometry distorts the spatial gravity signal, I compared gravity changes contoured from a hypothetical grid of points to gravity contoured from data at the station sites alone. In an ideal situation, a gravity survey would use a grid pattern of stations to minimize signal distortion, but rough volcanic terrain and considerations of survey time makes this virtually impossible at Kilauea. As Figure 7a illustrates, gaps in coverage can distort the spatial gravity signal. The top figure shows even coverage for a given source. The inflating source causes a given gravity change at each station, and when these gravity changes are contoured they create a smooth Mogi curve that peaks over the source. The bottom figure (7b) shows that when some of these stations are removed, even though the gravity change at the remaining stations is still the same, the gaps in coverage alter the contour of the data. Now instead of a high peak over the source, the apparent peak is shifted to the left and reduced in magnitude.

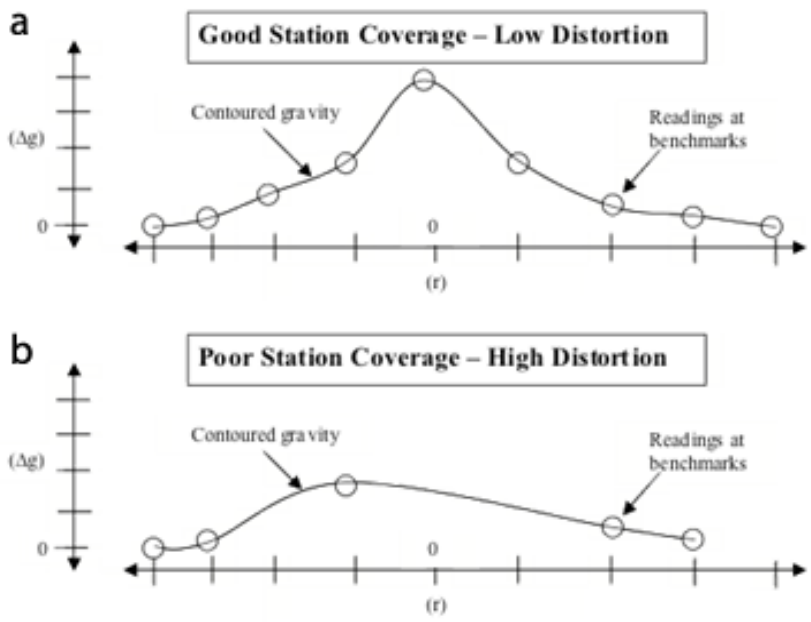

Figure 7. Schematic showing distortion of inferred gravity signal from poor station coverage. In the top figure, even station coverage allows contouring of gravity data to produce a smooth curve and provide a reliable indicator of source location (at r=0). In the lower figure, poor station coverage distorts the gravity signal when data is contoured, skewing the indication of source location.

To address this problem at Kilauea, I calculated the gravity change first for a hypothetical 500 by 500 grid of points and contoured the data to produce an ideal scenario. I also calculated gravity change at only the existing station locations, and contoured those data, using Matlab's "griddata" function and the default "v4" option. I then subtracted the grid-calculated map from the station-calculated map to obtain a map of the distortion, and calculated a numerical residual value between the two maps for a qualitative image of signal distortion. This method provides for a visual means of evaluating signal distortion, but lacks the quantitative results of an actual inversion. However, there are data in the calculated residual, so I deemed this method sufficient for this preliminary assessment of network capabilities.

Results

One method for assessing the network's ability to detect different sources is to keep track of how many stations are above the noise level for a range of different source depths and volumes. In Figure 8, I have plotted the number of stations above the noise level for intrusion simulations at each of the three sources. Each colored dot represents a scenario.

Source depth is plotted along the x axis, and source volume is plotted along the y axis with a base 10 logarithmic scale. The color of each dot corresponds to the number of stations above the noise level for that depth and volume combination. These dots are contoured for number of stations. The lowest line, which is dark blue, represents 5 stations above the noise level, and the highest, dark red, represents 45 stations above the noise level (there are 47 total stations in the current network). For all figures, the contours are parallel except at shallow depths, where they

diverge slightly because of station density close to the source. Figure 8a depicts detection threshold contours for a source at HMM, 8b at KEA, and 8c at SC.

From Figure 8a we can see that the network begins to detect a source at HMM at the 5 station level when it reaches just below $1x10^6$ m^3 in volume, and for 20 stations to detect a source at HMM, the source must be at least $6x10^6$ m^3. Sources at KEA are detectable by 5 stations when they reach $1.7x10^6$ m^3. Sources are detectable by 20 stations when they reach $6x10^6$ m^3, as at HMM (Figure 8b). Figures 8a and 8b show that the network is, for the most part, equally sensitive to sources at HMM and KEA.

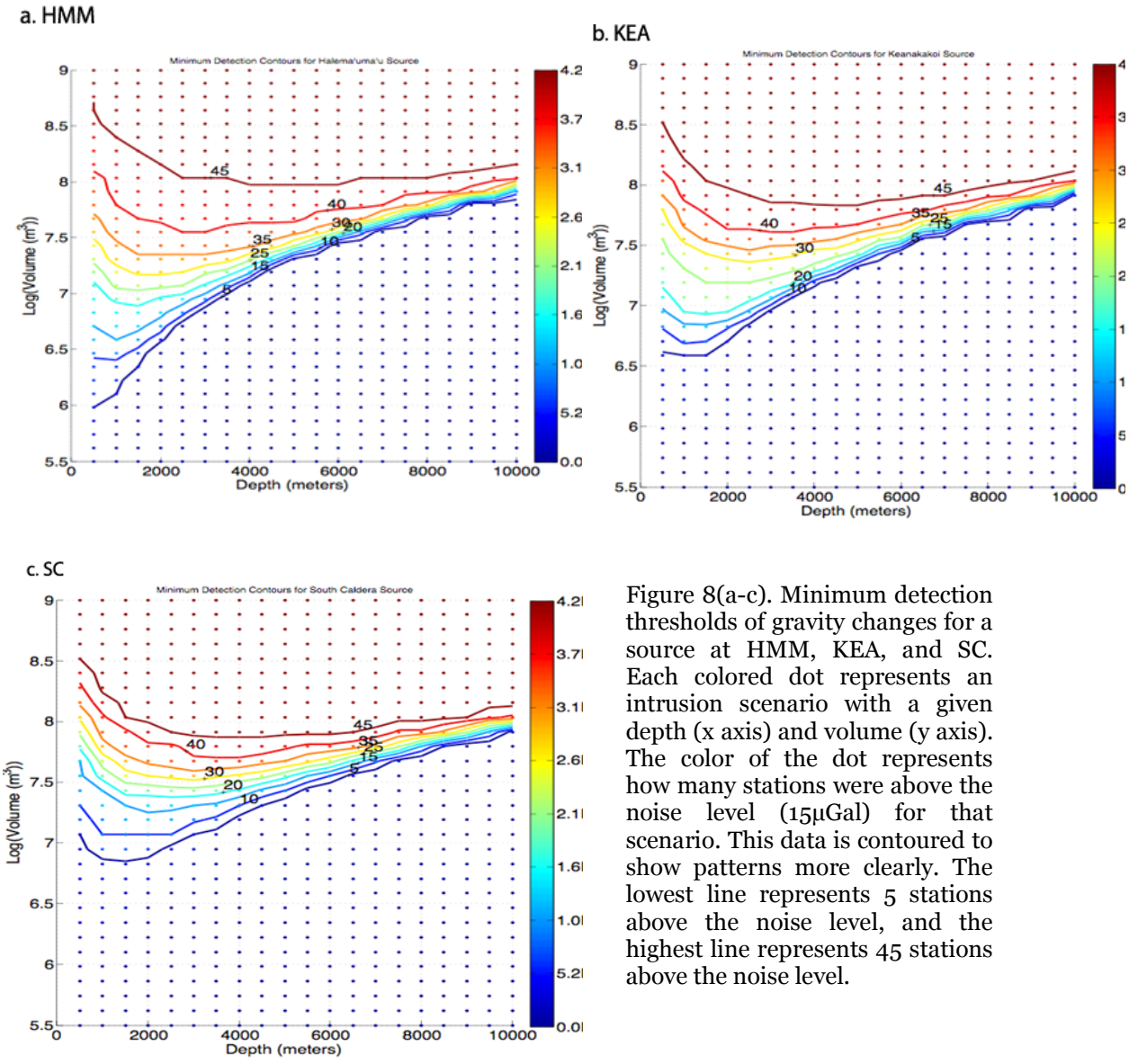

Figure 8(a-c). Minimum detection thresholds of gravity changes for a source at HMM, KEA, and SC. Each colored dot represents an intrusion scenario with a given depth (x axis) and volume (y axis). The color of the dot represents how many stations were above the noise level (15μGal) for that scenario. This data is contoured to show patterns more clearly. The lowest line represents 5 stations above the noise level, and the highest line represents 45 stations above the noise level.

Figure 8c shows that the network is much less sensitive to the SC source. A source of $6x10^6$ m^3 is necessary for a minimum of 5 stations to be above the noise level, whereas a source of this volume would be detectable by a minimum of 20 stations for a source at HMM or KEA (Figure

8a-b). For 20 stations in the network to detect a source at SC, the source needs to be at least 2.5×10^7 m^3.

Figure 8 shows that for all sources examined, the network will detect a source with a volume greater than 3×10^8 m^3 for all depths tested (this volume is slightly higher at HMM, at 5×10^8 m^3). For comparison purposes, the May 1973 east rift zone eruption produced 1.2×10^6 m^3 of lava, the 1977 east rift zone eruption produced 3.5×10^7 m^3, the July 1974 summit eruption produced 6.5×10^6 m^3, and the 1969 Mauna Ulu eruption produced 3.4×10^8 m^3 ("Global Volcanism Program," May 2011).

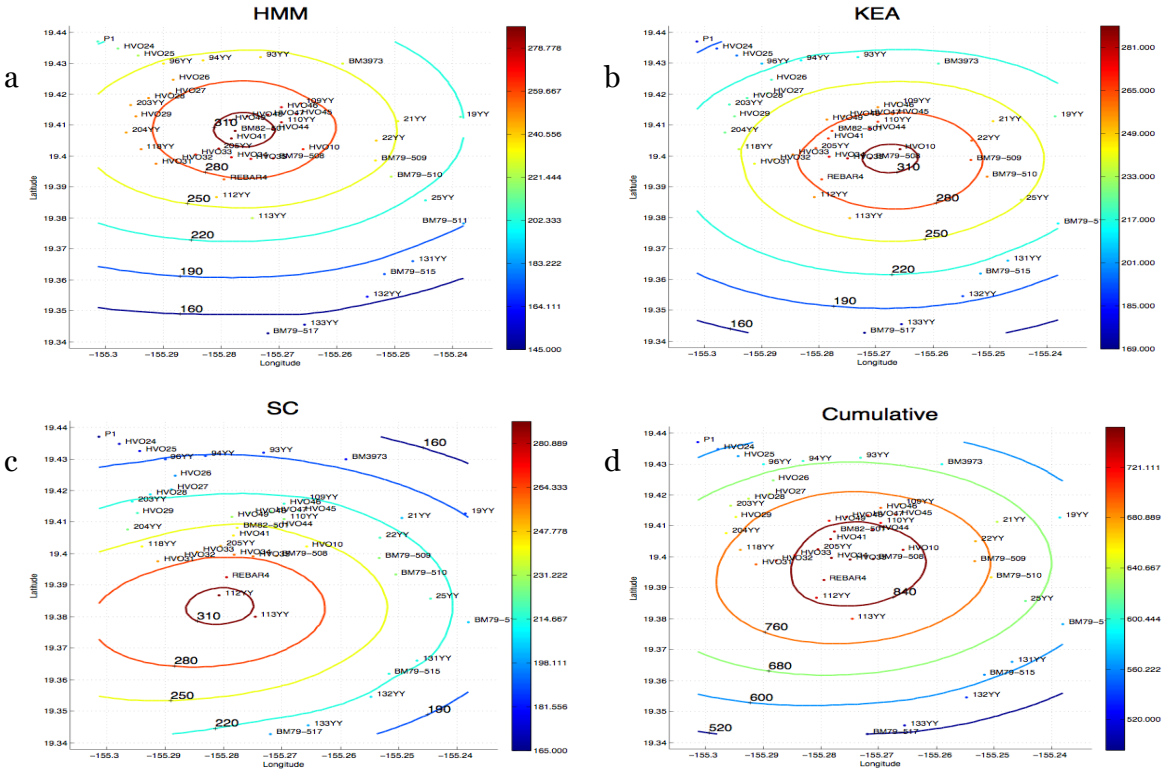

Figure 9(a-d). Relative station importance for detecting a source at HMM (a), KEA (b), and SC (d). Figure 9d is relative station importance using all three sources. Stations are plotted in their relative positions using latitude and longitude, and station color corresponds to the number of times that an individual station was above the noise level across all the scenarios (intrusions of different depths and volumes) calculated. Stations that fall within the third contour (80% BPV) are considered important to the network, and those that fall outside the third contour are less important to the network.

Figure 9a-d shows the relative importance of stations for a source at HMM, KEA, SC, and all sources combined, respectively. Each station is represented by a colored dot that represents relative station importance, with red colors representing stations with higher scores (meaning the station was above the noise level for more scenarios) and blue colors representing stations with lower scores. These dots are then contoured to show the spatial distribution of station importance. For a source at HMM, KEA, SC, and all sources cumulatively, the best possible values (BPVs) are 317, 313, 314, and 882, respectively, out of 600 simulations for the individual

sources, and 1800 simulations for the cumulative score (600 simulations for each of the three sources). The BPV for all sources is higher because this cumulative data set is the sum of the scores from the three individual sources.

Using the arbitrary definition that stations that score above approximately 80% of BPV are important and those that score less than 80% are less important, stations falling within the third highest contour in Figures 9 a-d are important (77-79% BPV), and those falling outside the third highest contour are less important. Figure 9a shows that the stations that are important for detecting a source at HMM are essentially inside the caldera, encompassing 32 of 47 total stations. Results for a source at KEA are similar (Figure 9b), with more stations to the east and south of the main caldera falling within the third contour and 26 stations total. Figure 9c shows that only 14 stations are important for detecting a source at SC, as only 14 stations fall within the third contour, and 12 of these are between the second and third contours. Looking at the cumulative map (Figure 9d), we see that stations in the caldera and directly outside of it are most useful, while stations along the Mauna Loa road (P1 to 96YY), the Hilina Pali road (BM79-511 to BM79-517), and Crater Rim Drive (94YY to 19YY) are less useful.

In summary, the network resolves sources at HMM and KEA fairly well, with little to no distortion of the signal. The source, however, shows considerable distortion. Figure 10 shows maps of residual for HMM (10a), KEA (10b), and SC (10c), al lcalculated for a source $5x10^7$ m^3 in volume and 2 km deep.

Stations are plotted in map view, and color SC corresponds to the residual between the grid calculated gravity map (the ideal network) and the station calculated map (the actual network). Reds are positive residual, blues are negative residual (the large negative residuals that occur on the edge of

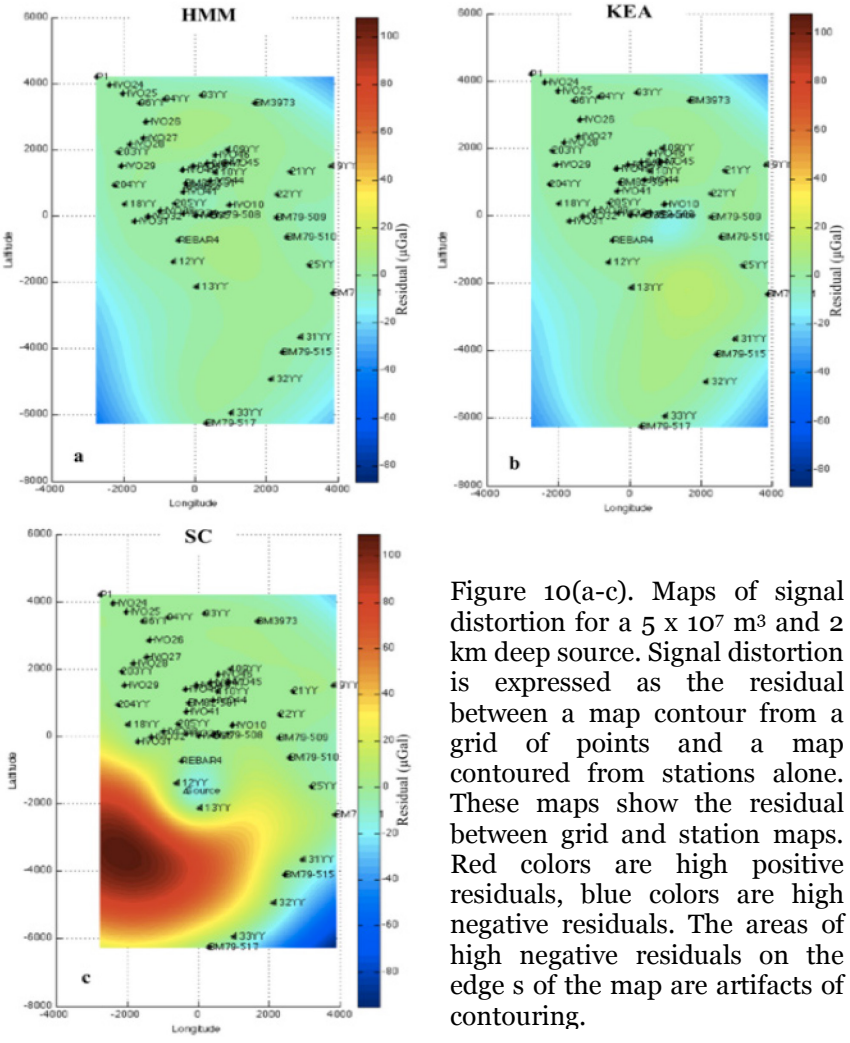

Figure 10(a-c). Maps of signal distortion for a 5 x 10^7 m^3 and 2 km deep source. Signal distortion is expressed as the residual between a map contour from a grid of points and a map contoured from stations alone. These maps show the residual between grid and station maps. Red colors are high positive residuals, blue colors are high negative residuals. The areas of high negative residuals on the edge s of the map are artifacts of contouring.

the map are an artifact of contouring). The maximum residual for the SC source is near 100 μGal (Figure 10c), whereas the residual for HMM and KEA is below 20 μGal (Figure 10a-b). These residuals increase as the source volume increases and/or depth decreases.

Figure 11 shows grid and station calculated maps for a HMM source of $5x10^7$ m^3 and 1 km depth (Figure 11a-b), and grid and station calculated maps for an SC source of $5x10^7$ m^3 and 2 km depth (Figure 11c-d). A shallower source at HMM (1 km) has a higher residual, but the spatial signal is not noticeably distorted between the grid map and the station map (Figure 11 a-b). In contrast, the spatial gravity signal from a source at SC is noticeably distorted between the grid map and the station map (Figure 11 c-d), spreading the circular Mogi signal in an oval that encompasses part of the southwest rift zone, an area of frequent volcanic activity.

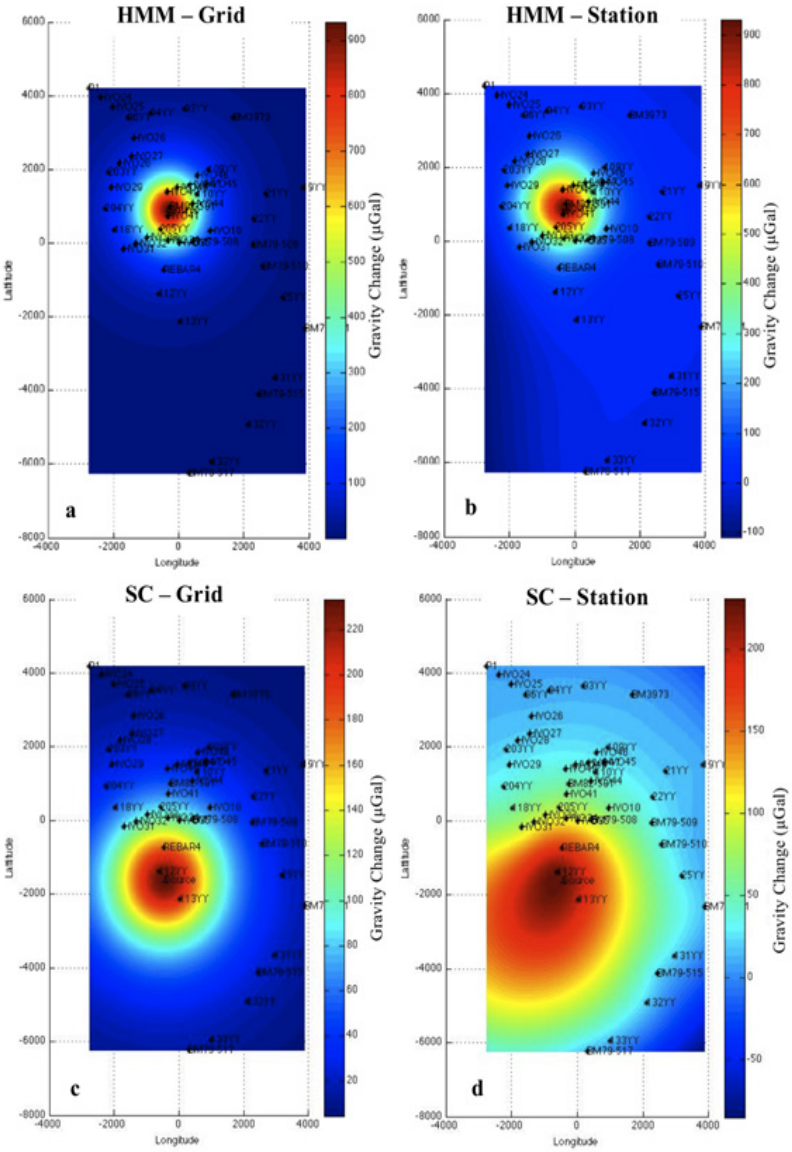

Figure 11 (a-d). Comparison of spatial gravity signal distortion between a source at HMM and a source at SC. Figures 11a and 11c show the ideal signal expected from a Mogi source. The ideal signal is created by calculating gravity at a hypothetical grid of points across the network area, and the n contouring the data produced by the grid of points. Figures 11b and 11d are produced by contouring only gravity changes calcuated at current sites, showing how the network does not appreciably distort the spatial gravity signal for a source at HMM, but causes significant distortion of a signal for source SC.

Discussion

The current network is able to detect most large intrusion volumes (>2x10^7 m^3) at depths less than 5 km, although smaller or deeper intrusions are less likely to be detected, especially at the SC source. For each source, detection criteria contour lines begin converging at deeper depths (Figure 8). This is because as the source gets deeper, the spatial gravity signal becomes longer wavelength, and the detection criteria saturates. This means that for each source, it will be difficult to establish a definite source location until the source is shallower than 8 km, because differences in gravity change between stations that would show source location may be obscured by the noise level of the instrument.

Conversely, at shallow depths these detection criteria contour lines are more widely spaced along the volume axis, because at shallower depths the signal is much more spatially localized (Figure 8), such that it takes larger volumes to make the small wavelength spatial gravity signal detectable at more stations. The spacing of the contours at shallow depths is a measure of station density around each source. For the HMM source, this spacing is fairly regular, indicating that stations are present at relatively uniform densities at all distances from the source (Figure 8a). By contrast, for the SC source, the contours for 5, 10, and 15 stations are very widely spaced and the higher contours are more closely spaced (Figure 8c). This reflects very sparse station coverage near the source, and denser coverage farther away from it. This means that a source must be larger than 1.7x10^7 m^3 before it can be detected beyond the few stations close to the SC source. The KEA source is somewhere in between HMM and SC; its lower contour lines are densely spaced and its higher contour lines are more widely spaced (Figure 8b). However, the closely spaced lower contour lines ensure that smaller sources can be reliably detected by numerous stations.

Most of the detection level contours reach a local minimum at some depth and volume combination, meaning that for a given volume, the same level of detection (say, 20 stations) is possible for two different depths. This is because of the change in the shape of the Mogi model signal with depth: for a constant volume, at shallow depths the signal peaks sharply, and at greater depths, the signal peak spreads out. This means that at certain detection level (the contours on the figure), for a given volume there is an optimum depth for detection. For example, an HMM source of 10^7 m^3 will be detected by 25 stations at 1.5 km depth, but will only be detected by 20 stations at 0.75 km depth.

The results from the station value maps are encouraging. For all stations evaluated cumulatively, 33 of 47 total stations are important to the network, scoring above 680 (which is 77% of BPV) (Figure 9d). The stations that fall outside of 81% BPV are typically the less easily accessible stations (the stations along Mauna Loa Road and the Hilina Pali Road, and 19YY) or less reliable stations (93YY, 94YY, and BM3973). Interestingly, P1, the base station, does not have the lowest score, which suggests that for very large or very shallow events P1 may not be an ideal base station (figure 9d). Stability of the benchmark and accessibility are other considerations for choosing base stations. Conversely, the stations that score lower than P1 may not require frequent surveying. Continuous gravimeters could be placed in areas of greatest station value for each of these three possible sources to maximize effectiveness.

My analysis also suggests that it might be useful to prioritize surveys for different coverage areas and different time intervals. It takes about 1.5 weeks to survey the entire current network, but it would only take 1-2 days to survey all the stations inside the first contour on the cumulative station value map (Figure 9d). Surveying all the stations within the third contour in Figure 9d would probably take 5-6 days. A potential survey schedule could be a yearly survey of the entire network, a survey of third contour stations every 3 to 4 months, and a survey of the first contour stations every 1 to 2 months.

The station value maps for each of the three sources (Figure 9 a-c) suggests that the network is best configured for sources at HMM and KEA. These maps also suggest that the network is not as well set up for a source at SC, a fact that is troubling since this area has shown marked deflation and gravity decreases in recent leveling and gravity surveys (Johnson et. al. 2010). Only 14 stations are important for this source, as compared to HMM and KEA, which have 32 and 26 important stations, respectively.

Once I had determined through forward modeling that the south caldera region showed the greatest degree of bias from the current station network, I used forward modeling to determine possible new station locations and assess their potential for improving the residual error. I began with a map of current leveling stations superimposed on the map of existing stations, and chose new trial station locations based on which of these leveling stations I knew to be accessible by road (or nearly so). Figure 12 shows the trial station locations I chose.

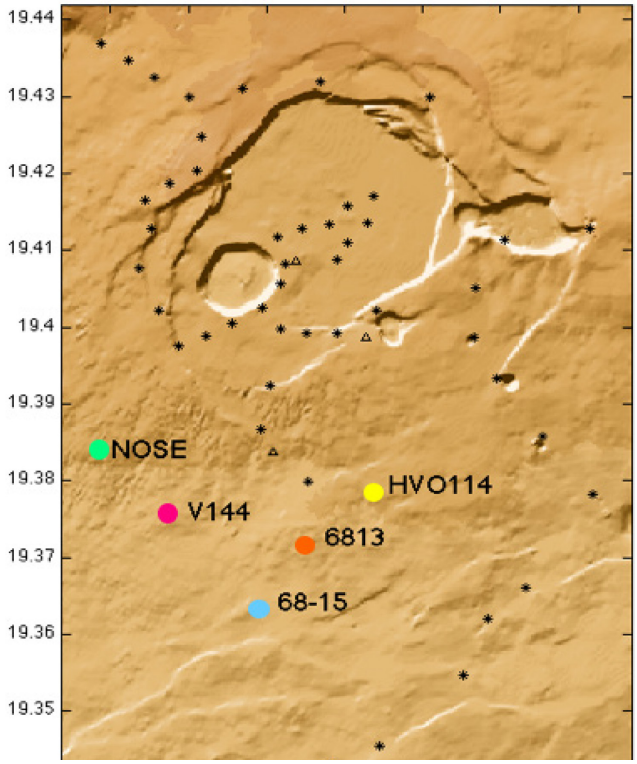

Figure 12. Proposed locations for new gravity stations. These sites are co-located with existing leveling benchmarks (see figure 3). Stations in the existing network are marked with stars, and source locations are marked with triangles. (x-axis is latitude, y-axis is longitude).

I then optimized station order by first trying only one station, then seeing which station of the five possibilities gave the greatest improvement in residual. Then, using the best station of those five as the first station, I would then try two stations, and find which of the remaining four gave the greatest improvement, and use these two best stations when trying three stations, and so on, until I had determined the best order for station addition. Figure 13 shows several alternate station orders, plotting percent residual improvement as a function of number of stations added. Table 1 shows the order in which stations were added for station orders A through F. Figure 13 shows that adding stations using order A (V144, 6813, HVO114, NOSE, 68-15) gives residual improvement the fastest with each station added.

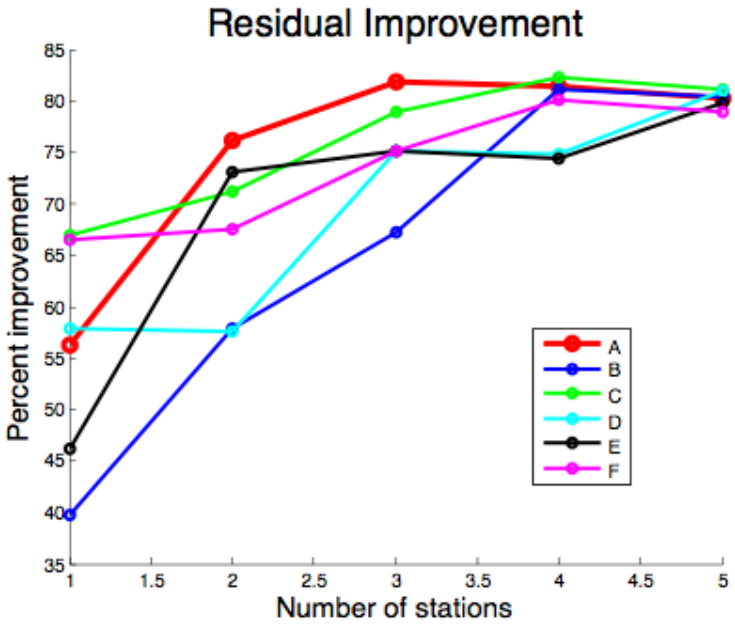

Figure 13. Plot of percent residual improvement versus number of stations added for a variety of station orders. Although some orders (C,D, and F) have a greater improvement than order A initially, these other orders do not improve as fast as A after this first point. Order A shows the greatest improvement fastest, and is therefore the optimal order for adding new stations to the network.

Table 1. Table showing the order of stations in each order in Figure 13

Station Orders

Order name	1st station	2nd station	3rd station	4th station	5th station
A	V144	68-13	HVO144	NOSE	68-15
B	NOSE	V144	HVO114	68-13	68-15
C	68-15	NOSE	HVO114	68-13	V144
D	V144	NOSE	68-13	68-15	HVO114
E	68-13	NOSE	V144	68-15	HVO114
F	68-15	V144	68-13	HVO114	NOSE

a

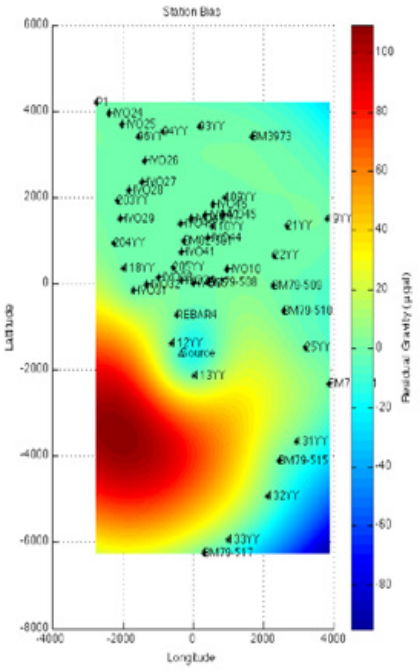

0 new stations

b

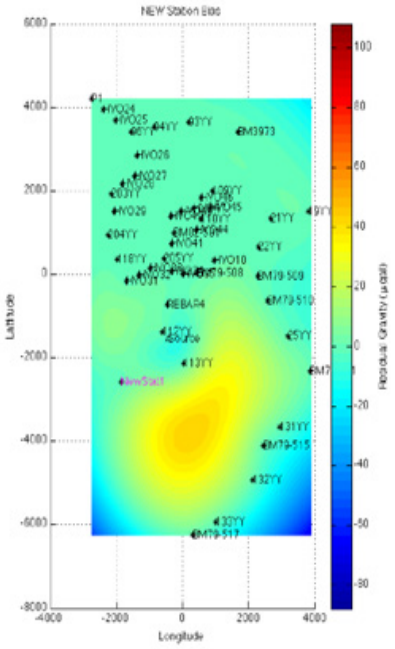

1 new station

c

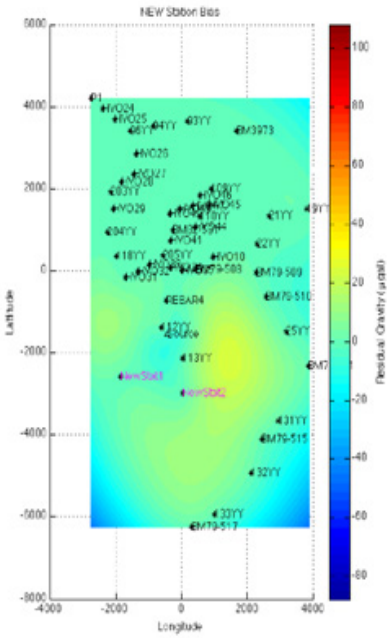

2 new stations

d

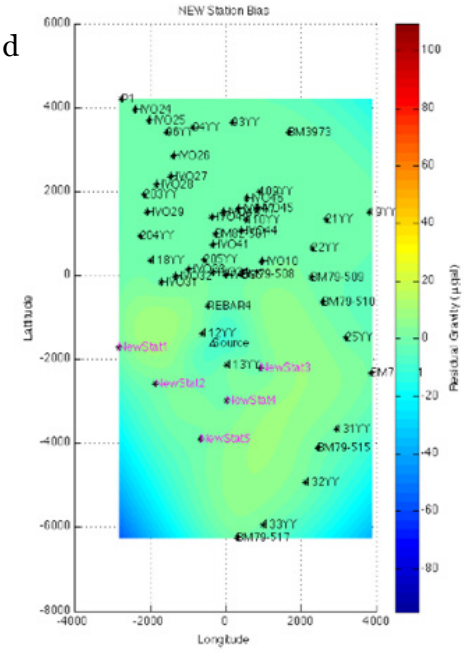

3 new stations

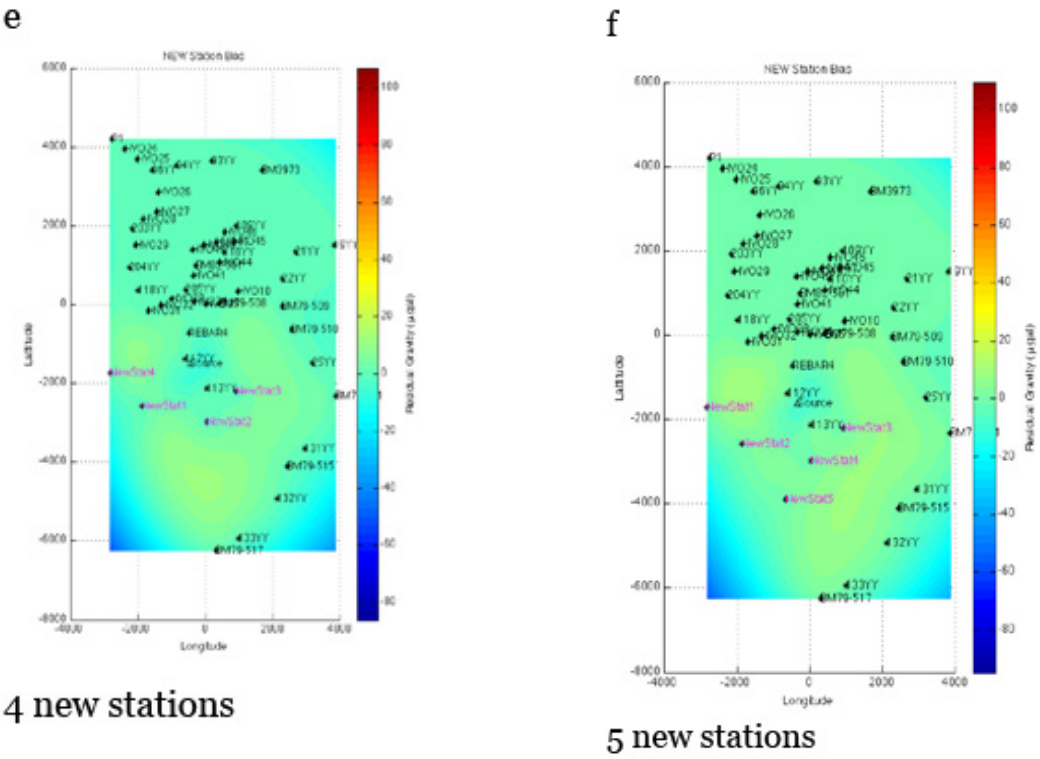

Figure 14(a-f): Maps of improving residual with the addition of new stations in the south caldera area. These maps represent the difference between a map of gravity change contoured using a grid of points and a gravity map calculated using data points only at station locations. High positive residual is in red, and high negative residual is in blue (the high negative residual on the edges of the maps is an artifact of the contouring). Figures a-d show dramatic improvement, but figures d-f show little change.

In general, there is dramatic improvement in the residual for the first three stations added, but after this the reductions in the residual seem to level off or decrease slightly (Figure 14). Figure 14 shows maps of residual after 0-5 stations have been added. The difference between Figure 14a (zero new stations), and Figure 14d (three new stations) is dramatic – with no new stations, residual reaches nearly 100 μGal, but with three additional stations in the south caldera area, maximum residuals drop to below noise levels (below 15μGal). However, there is little difference between Figures 14d-f (four and five new stations), where maximum residuals remain at around the same level. Future work should include a more comprehensive set of possible sources. These sources could include locations on the east and southwest rift zones, and also northeast of Halema`uma`u crater in the caldera. It would also be very useful to forward model from existing real data to see how the current network and any proposed alterations to the current network would detect gravity change in more realistic situations. Using inverse methods would better quantify network distortion and improvements to the distortion through the addition of new stations. Also important would be additional forward modeling to determine how well the network could detect vesiculation of existing intrusions.

Conclusions

Using campaign gravity surveys to track subsurface changes in mass is a useful technique for monitoring Kilauea's constant activity. Since eruptions at Kilauea are often preceded by intrusions of magma at the summit, gravity surveys can effectively track this subsurface activity long before surface activity commences, providing longer warning time for purposes of hazard mitigation (Decker, 1987; Johnson, 1987). Campaign gravity surveys can provide good spatial coverage, and additional continuous meters, carefully placed, can provide good temporal coverage (Battaglia et al., 2008).

However, this monitoring technique is useful as long as the data it provides is of good quality. Forward modeling magma intrusions using a simple point source model is an effective way to understand the capabilities and limitations of the campaign gravity network on Kilauea. Although a vast simplification of a much more complicated reality, these models give the researcher a first look at what the network can detect, which stations are most important to the network, and where the network needs additional station coverage.

The current gravity network on Kilauea's summit is well suited for detecting sources at HMM or KEA, and by extension any sources within the caldera. However, with the current network configuration, sources in the SC area are much harder to detect and locate. Installing new stations in this area would greatly alleviate this problem; in fact, only three new stations may be necessary. To simplify future gravity surveys, some stations from the current network (HVO24–96YY, 94YY–19YY, and BM79-511–BM79-517) could be surveyed less frequently, as this forward modeling shows that they are of lesser importance to the network. Conversely, some stations (mostly those in the caldera along the Chain of Craters Road) could be surveyed with greater frequency based on their importance to detecting likely sources.

Acknowledgements

I would like to thank Kathy Cashman, David Schmidt, and Michael Poland for their extensive help and patience during research and writing. I would also like to thank Michael Poland and everyone else at the Hawaiian Volcano Observatory for the incredible volunteering opportunity that served as the inspiration for this work. Furthermore, thank you to everyone at the University of Oregon, especially the Department of Geological Sciences, for creating such a wonderfully encouraging and supportive environment that allows this kind of work to happen at the undergraduate level.

References

Battaglia, M., Gottsmann, J., Carbone, D., Fernández, J. (2008). "4D volcano gravimetry." *Geophysics,* 73, 3-18.

Battaglia, M., Roberts, C., & Segall, P. (1999). Magma intrusion beneath long valley caldera confirmed by temporal changes in gravity. *Science, 285*. 2119-2122.

Camacho, A.G., Fernandez, J., Charco, M., Tiampo, K.F., Jentzsch, G. (2007). "Interpretation of 1992-1994 Gravity Changes around Mayon Volcano, Philippines, Using Point Sources." *Pure & Applied Geophysics, 127*, 733-749.

Daniele, D., Budetta, G., Greco, F., Zuccarello, L. (2007). "A data sequence acquired at Mt. Etna during the 2002-2003 eruption highlights the potential of continuous gravity observations as a tool to monitor and study active volcanoes." *Journal of Geodynamics 43,* 320-329.

Decker, R.W. (1987). United States. *Dynamics of Hawaiian Volcanoes: An Overview*. Washington: United States Government Printing Office.

Dzurisin, D. (2007). *Volcano Deformation: Geodetic Monitoring Techniques*. Chichester, UK: Praxis Publishing.

Ewert, J.W., Guffanti, M., Murray, T.L. (2005). An Assessment of Volcanic Threat and Monitoring Capabilities in the United States: Framework for a National Volcano Early Warning System: U.S. Geological Survey Open-File Report 2005-1164.

Fee, D., Garcés, M., Patrick, M., Chouet, B., Dawson, P., Swanson, D. (2010). "Infrasonic harmonic tremor and degassing bursts from Halema'uma'u Crater, Kilauea Volcano, Hawaii." *Journal of Geophysical Research*, *115*.

Fiske, R. S., Rose, T.R., Swanson, D., Champion, D., and McGeehin, J. (2009). "Kulanaokuaiki Tephra (ca. A.D. 400–1000): Newly recognized evidence for highly explosive eruptions at Kīlauea Volcano, Hawai'i." *GSA Bulletin*, *121*, 712-728.

"Global Volcanism Program: Kilauea: Eruptive History." *Global Volcanism Program*. Smithsonian National Museum of Natural History, n.d. Web. 31 May 2011.

Gottsmann, J., Berrino, G., Rymer, H., Williams-Jones, G. (2003). "Hazard assessment during caldera unrest at the Campi Flegrei, Italy: a contribution from gravity-height gradients." *Earth and Planetary Science Letters, 211*, 295-309.

Houghton, B.F., Swanson, D., Carey, R.J., Rausch, J., Sutton, A.J. (2011). "Pigeonholing Pyroclasts: Insights from the 19 March 2008 Explosive eruption of Kilauea Volcano." *Geology, 39*, 263–266.

"HVO Kilauea Status Page." *Hawaiian Volcano Observatory*. USGS, 31 May 2011. Web. 31 May 2011.

Jaggar, T. A., Finch, R.H. (1924). "The explosive eruption of Kilauea in Hawaii, 1924." *American Journal of Science, 8*, 353-374.

Johnson, D. J., Eggers, A.A., Bagnardi, M., Battaglia, M., Poland, M., Miklius, A. (2010). "Shallow magma accumulation at Kilauea Volcano, Hawai'i, revealed by microgravity surveys." *Geology*, *38*, 1139-1142.

Johnson, D. J. (1992). "Dynamics of Magma Storage in the Summit Reservoir of Kilauea Volcano, Hawaii." *Journal of Geophysical Research*, *97*, 1807-1820.

Jousset, P., Dwipa, S., Beauducel, F., Duquesnoy, T., Diament, M. (2000). "Temporal gravity at Merapi during the 1993 – 1995 crisis: an insight into the dynamical behaviour of volcanoes." *Journal of Volcanology and Geothermal Research, 100*, 289 – 320.

Poland, M. P., Sutton, J., Gerlach, T.M. (2009). "Magma Degassing Triggered by static decompression at Kilauea Volcano, Hawai`i." *Geophysical Research Letters, 36*, L16306.

Sutton, J., Elias, T., Hendley, J.W. II., Stauffer, P.H. (2000). United States. *Volcanic Air Pollution—A Hazard in Hawai`i*. Web. 31 May 2011. <http://pubs.usgs.gov/fs/fs169-97/>.

Swanson, D.A. (2008). "Hawaiian oral tradition describes 400 years of volcanic activity at Kīlauea." *Journal of Volcanology and Geothermal Research*, *176*, 427-431.

Williams-Jones, G., Rymer, H., Rothery, D.A. (2003). "Gravity changes and passive SO_2 degassing at the Masaya caldera complex, Nicaragua." *Journal of Volcanology and Geothermal Research, 123*,137-160.

Williams-Jones, G., Rymer, H., Mauri, G., Gottsmann, J., Poland, M., Carbone, D. (2008). "Toward continuous 4D microgravity monitoring of volcanoes." *Geophysics, 73*, 19-28.